Investigation on the intensity noise characteristics of the semiconductor ring laser*

Kang Ze-Xin(康泽新)[a)b)†], Cai Xin-Lun(蔡鑫伦)[b)], Wen Xiao-Dong(温晓东)[a)], Liu Chao(刘 超)[a)], Jian Shui-Sheng(简水生)[a)], and Yu Si-Yuan(余思远)[b)]

[a)] *Key Laboratory of All Optical Network & Advanced Telecommunication Network of EMC, Institute of Lightwave Technology, Beijing Jiaotong University, Beijing* 100044, *China*

[b)] *The Department of Electrical and Electronic Engineering, University of Bristol, Bristol, BS*8 1*TR, UK*

(Received 27 February 2013; revised manuscript received 17 June 2013; published online 10 December 2013)

Based on the frequency-domain multimode theoretical model, detailed investigations on the noise characteristic of the semiconductor ring laser (SRL) are first performed in this paper. The comprehensive nonlinear terms related to the third order nonlinear susceptibility χ^3 are included in this model; the Langevin noise sources for electric field and carrier density fluctuations are also taken into account. As the injection current increases, the SRL may present several operation regimes. Remarkable and unusual low frequency noise enhancement in the form of a broad low frequency tail extending all the way to the relaxation oscillation peak is observed in any of the operation regimes of SRLs. The influences of the backscattering coefficient on the relative intensity noise (RIN) spectrum in typical operation regimes are investigated in detail.

Keywords: semiconductor ring laser, relative intensity noise, low frequency noise enhancement

PACS: 42.55.Px, 42.60.Mi, 42.65.Pc **DOI:** 10.1088/1674-1056/23/2/024203

1. Introduction

Semiconductor ring lasers (SRLs) are promising devices for optoelectronic integrated circuits (OEIC) as they possess many incomparable advantages compared with conventional FP or DFB lasers,[1,2] such as small footprint and simple fabrication due to the absence of cleaved facets, cost-saving and versatility attributed to the bidirectional operation, and high spectral purity arising from the natural property of a travelling wave.

Sorel *et al.*[3,4] observed several working regimes in SRLs, including the bidirectional continuous wave (bi-CW), the bidirectional continuous wave with alternate oscillations (bi-AO) and the bi-stable unidirectional continuous wave (bi-UNI). It should be noted that the above calculation progress was based on the two-mode model. In order to clearly explain the nonlinear dynamical characteristics of SRLs, such as mode-hopping and asymmetric frequency spectrum, it is necessary to extend the two-mode model to the multimode model and take the third order nonlinear susceptibility χ^3 in to rate the equations. Subsequently, Cai *et al.*[5] verified these novel operating regimes in SRL using the frequency domain multimode model.

SRLs are employed as light sources in the fiber optical communication systems and are used as photonic switching devices in wavelength switched networks.[6,7] The performances of these OEIC systems are often critically affected by the relative intensity noise (RIN) of the source laser. It is, therefore, of great interest to characterize the RIN properties of SRLs. Quantum noise due to spontaneous emission is the fundamental noise in a semiconductor laser. On account of the intrinsic nature of the semiconductor laser, the noise cannot be eliminated completely but it can be reduced to the lowest level. Besides the fundamental quantum noise, there is another type of non-negligible noise called partition noise in the multimode semiconductor laser, especially in SRL. Both of them can induce the fluctuation of the optical field intensity, which is technically characterized by the so-called RIN accounting for the signal-to-noise ratio (SNR).

Compared with other types of semiconductor lasers, such as the distributed feedback (DFB) laser, the distributed Bragg reflective (DBR) laser and the Fabry–Pérot (FP) laser,[8–10] the SRL exhibits a very remarkable feature of the RIN spectra: low frequency noise enhancement in the form of a broad low frequency tail extending all the way to the relaxation oscillation peak. This low-frequency noise enhancement is expected to appear in all types of ring geometries, such as circular and triangular geometries. Ji *et al.*[11] have observed experimentally and verified theoretically the remarkable low-frequency noise enhancement in the RIN spectra of the triangular geometry SRL. However, the fabrication of three turning mirrors in the triangle-shaped ridge waveguide structure increases the difficulty in fabricating the integrated chip. Therefore, in the actual OEIC systems, the circular or the race-track geometry SRLs may attract more attention due to their simple fabrication. As for the circular ring geometry, Mikroulis *et al.*[12] did some research on the enhanced low frequency RIN; however,

*Project supported by the Major State Basic Research Development Program of China (Grant No. 2010CB328206).

†Corresponding author. E-mail: newism@hotmail.com

© 2014 Chinese Physical Society and IOP Publishing Ltd

the nonlinear mechanism employed in their model was based on Refs. [13] and [14], where the four-wave mixing (FWM) and carrier diffusion (CD) effects, which are indispensable in analyses of SRLs' dynamics, were not included. The CD effect is significant in semiconductor lasers, SRL in particular, as it strongly influences the carrier distribution (further affects the gain and the refractive index) spatiotemporally originating from the beating of counter propagating modes. Due to this spatiotemporal modulation, the grating visibilities for co-propagation modes and counter-propagation modes are different in SRLs. Further, the backscattering coefficient, which proved to be a critical parameter for the performance of SRL, was not taken into consideration. Antonio *et al.*[15] have analytically investigated the influence of the backscattering coefficient on the noise spectrum of SRL based on a two-mode model. However, as is well known, the two-mode model has some inherent limitations itself and is not a perfect model to investigate the characteristics of SRL, such as its incapability of interpreting the mode-hopping phenomenon and the asymmetric frequency spectrum.

In this paper and for the first time, the comprehensive frequency-domain multimode model is implemented to investigate the RIN properties of circular geometry SRL. The detailed expression for χ^3 is derived from density matrix theory by taking into account the effects of carrier density pulsation (CDP), spectral hole burning (SHB) and carrier heating (CH),[5,16–18] and introducing the carrier diffusion (CD).[5,18] The requisite Langevin noise sources[19,20] for electric field and carrier density fluctuations are also taken into consideration. In the following, we focus on the typical bi-AO and bis-UNI regimes of SRL to investigate the influence of the backscattering coefficient on the RIN property. To the best of our knowledge, no such systematic analysis of the influence of backscattering on the RIN characteristic has been performed.

2. Theoretical analysis

A schematic diagram of the SRL is illustrated in Fig. 1. Both the output waveguides are tilted to avoid the reflections from the connecting facets of both sides. Therefore, in the calculation, the optical feedbacks from connecting parts are ignored. The total electric field inside the laser cavity can be expressed as the sum of electric fields of all resonant modes

$$E(t) = \sum_i E_i(t)\,\mathrm{e}^{-\mathrm{j}\omega_i t}, \tag{1}$$

where E_i is the mean-field slowly varying complex amplitude of the electric field for the i-th mode at optical angular frequency ω_i, with i covering all the CW modes and CCW modes in the SRL. Ignoring the influence of dispersion, the mode space is assumed to be $\Delta\omega$ equally. We consider an odd number $2T+1$ of modes for each direction ($4T+2$ totally) in the SRL. The CW/CCW modes are extended to both the positive and the negative directions from the central mode labelled by $M=0$ and are distinguished by the positive number M ($M>0$) denoting the long-wavelength side and negative number M ($M<0$) denoting the short-wavelength side, M counts from $-T$ to T.

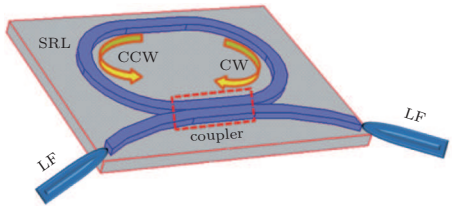


Fig. 1. (color online) The schematic illustration of an SRL. The tilted output waveguides are designed to avoid the reflections from the connecting facets of both sides. LF: lensed fiber; CW: clockwise mode; CCW: counterclockwise mode.

Under slowly varying envelope approximation, the time evolution of the electric field amplitude E_i in the semiconductor laser cavity can be described by the following equation, which was firstly introduced to describe the nonlinear dynamics of SRLs by Born *et al.* in Ref. [16]:

$$\begin{aligned}\frac{\mathrm{d}E_i}{\mathrm{d}t} &= \frac{1}{2}\frac{c}{n_\mathrm{g}}\Gamma\left[g(N,\omega_i) - \mathrm{j}\alpha\Delta N a\right]E_i - \frac{1}{2}\frac{E_i}{\tau_\mathrm{p}} \\ &\quad + \frac{1}{2}\frac{\omega_i\Gamma}{n_i n_\mathrm{g}}\sum_{lmn}\chi^{(3)}_{lmn}E_l E^*_m E_n - K_\mathrm{BSR}E_{-i} + F_{E_i}(t). \end{aligned}\tag{2}$$

Here, we take the Langevin noise source $F_{E_i}(t)$ into consideration.

The first term on the right-hand side of Eq. (2) represents the linear gain and frequency shift of the i-th mode, c is the light velocity in a vacuum, n_g is the corresponding group index, Γ is the confinement factor, ΔN denotes the deviation of the carrier density from the threshold value, a is the material differential gain coefficient and α is the linewidth enhancement factor. The linear gain is given by a "piecewise-quadratic" frequency-dependent relation as follows:

$$\begin{aligned} &g(N,\omega_i) = a(N-N_0) - b(\omega_i-\omega_0)^2, \\ &b = \begin{cases} b_1, & \omega_i \leqslant \omega_0, \\ b_2, & \omega_i > \omega_0, \end{cases} \end{aligned}\tag{3}$$

where N represents the transparency carrier density and b denotes the linear gain dispersion coefficient. ω_0 refers to the central angular frequency of the linear gain that is assumed to be 155 nm.

The second term is the optical loss experienced by the i-th mode; τ_p is the photon lifetime and expressed as

$$\tau_\mathrm{p} = \left[\frac{c}{n_\mathrm{g}}\left(\gamma + \frac{1}{L}\ln\frac{1}{T_1}\right)\right]^{-1}, \tag{4}$$

with γ being the internal loss, L the active length and T_1 the coupling transmission ratio.

The third term describes the nonlinear contribution to the evolution of an electric field, n_i denotes the refractive index of mode i, χ^3_{lmn} refers to the third order susceptibility and is given by the following expression:

$$\chi^3_{lmn} = \chi^{\mathrm{N}}_{lmn}(\Omega_{mn}) + \chi^{\mathrm{ch}}_{lmn}(\Omega_{mn}) + \chi^{\mathrm{shb}}_{lmn}(\Omega_{mn}), \quad (5)$$

$$\chi^{\mathrm{N}}_{lmn}(\Omega_{mn}) = -\Pi\varepsilon_N\eta^{\mathrm{N}}(\alpha+j) \times \frac{1}{(1-\mathrm{j}\Omega_{mn}\tau_N\eta^{\mathrm{N}})(1-\mathrm{j}\Omega_{mn}\tau_1\eta^1)}\chi_0^{1''}, \quad (6)$$

$$\chi^{\mathrm{ch}}_{lmn}(\Omega_{mn}) = -\Pi\varepsilon_{\mathrm{ch}}\eta^{\mathrm{ch}}(\alpha_{\mathrm{ch}}+j) \times \frac{1}{(1-\mathrm{j}\Omega_{mn}\tau_{\mathrm{ch}}\eta^{\mathrm{ch}})(1-\mathrm{j}\Omega_{mn}\tau_1\eta^1)}\chi_0^{1''}, \quad (7)$$

$$\chi^{\mathrm{shb}}_{lmn}(\Omega_{mn}) = -\Pi\varepsilon_{\mathrm{shb}}\eta^1\frac{j}{1-\mathrm{j}\Omega_{mn}\tau_1\eta^1}\chi_0^{1''}, \quad (8)$$

$$\Pi = \frac{2\varepsilon_0 n_0 n_{\mathrm{g}}}{nh\omega_0}, \quad (9)$$

$$\chi_0^{1''} = -\frac{n_i c}{\omega_i}g(N,\omega_i), \quad (10)$$

where τ_{N}, τ_{ch}, and τ_1 are the differential carrier lifetime, electron carrier heating time and intra-band relaxation time respectively. ε_{N}, $\varepsilon_{\mathrm{ch}}$, and $\varepsilon_{\mathrm{shb}}$ denote the nonlinear coefficients associated with CDP, CH and SHB. α_{ch} is the linewidth enhancement factor for CH. $\Omega_{mn} = \omega_n - \omega_m$ is the beat frequency. η^{N}, η^{ch}, and η^1 are the grating visibility due to the carrier diffusion.

The fourth term indicates the intra-cavity backscattering between counter-propagating modes and the backscattering rate $K_{\mathrm{BSR}} = k_{\mathrm{d}} + \mathrm{i}k_{\mathrm{c}}$, where k_{d} is the dissipative coupling and k_{c} is the conservative coupling between counter-propagating modes.

Equation (2), together with the following equation for the carrier density, could describe the dynamics of SRL. Taking the Langevin noise source $F_N(t)$ into account, the equation for carrier density can be expressed as[16]

$$\frac{\mathrm{d}N}{\mathrm{d}t} = \frac{I}{eV} - \frac{N}{\tau_{\mathrm{s}}} - \sum_i g(N,\omega_i)\times\left(\frac{2\varepsilon_0 n_{\mathrm{g}} n_i}{n\omega_i}|E_i|^2\right) + F_N(t), \quad (11)$$

where e is the electron charge, V the volume of the active region and τ_{s} is the carrier lifetime, given by

$$\tau_{\mathrm{s}}^{-1} = A + BN + CN^2, \quad (12)$$

with A, B and C being the non-radiative, radiative and Auger recombination coefficients, respectively.

Functions F_E(t) and F_N(t) are both the Langevin noise sources of a Gaussian type with zero means, which satisfy the following cross-correlations:[19–21]

$$\langle F_{E_m}(t)F_{E_n}(t')\rangle = V_{E_mE_n}\delta_{mn}\delta(t-t'), \quad (13)$$

$$\langle F_N(t)F_N(t')\rangle = V_{NN}\delta(t-t'), \quad (14)$$

$$\langle F_{E_m}(t)F_N(t')\rangle = V_{E_mN}\delta_{mn}\delta(t-t'), \quad (15)$$

where δ is Dirac's delta function. These random numbers are introduced into the rate equations to account for the optical quantum noises associated with the spontaneous emission. The values of corresponding variable V_{xy} (x and y referring to the denotations E_m and N) are calculated from the assumed quasi-steady state solutions E_i and N of Eqs. (2) and (11). After derivation, we can obtain

$$F_{E_m}(t_i) = \sqrt{\frac{a\Gamma N(t_{i-1})}{2VT_{\mathrm{c}}(t_i - t_{i-1})}}(g_r + \mathrm{j}g_i), \quad (16)$$

$$F_N(t_i) = \sqrt{\frac{V_{NN}(t_i) + \sum_m \frac{a\Gamma}{V}T_{\mathrm{c}}|E_m(t_{i-1})|^2\frac{N_u^2}{N(t_{i-1})}}{\Delta t}}g_N + \sum_m\sqrt{\frac{a\Gamma T_{\mathrm{c}}}{2\Delta tV}}N_u|E_m(t_{i-1})|(g_r+\mathrm{j}g_i), \quad (17)$$

$$N_u = N(t_{i-1}) + bV(\omega_i - \omega_0)^2 + N_{\mathrm{g}}, \quad (18)$$

$$T_{\mathrm{c}} = \frac{2\varepsilon_0 n_i n_{\mathrm{g}}}{\hbar\omega_i}, \quad (19)$$

where g_r, g_i, and g_N are the independent Gaussian white random numbers with variances of unity and zero mean values. The Gaussian noise sources $F_{E_m}(t_i)$ and $F_N(t_i)$ satisfying the relations (13)–(15) at each t_i are generated for the simulation.

The most important analyses of noise characteristics are based on the small signal analysis introduced into the semiconductor laser by Haug.[22] In our presented numerical approach, the RIN characteristics can be specified with the power spectral density (PSD) of the RIN as a function of noise frequency, which can be calculated from the following expressions:

$$\delta P(t) = P(t) - \overline{P}, \quad (20)$$

$$\mathrm{RIN} = \frac{1}{\overline{P}^2}\left\{\frac{1}{T}\int_0^T\left[\int_0^\infty \delta P(t)\delta P(t+\tau)\mathrm{e}^{\mathrm{j}\omega\tau}\mathrm{d}\tau\right]\mathrm{d}t\right\} = \frac{1}{\overline{P}^2}\left\{\frac{1}{T}\left|\int_0^T\delta P(\tau)\mathrm{e}^{-\mathrm{j}\omega\tau}\mathrm{d}\tau\right|^2\right\} = \frac{1}{T\overline{P}^2}\left|\Delta t\cdot FFT\{\delta P(t)\}\right|^2, \quad (21)$$

where $\bar{P}$ is the mean power of all modes, FFT the fast Fourier transform, $\delta P(t)$ the power fluctuation with zero mean value and Δt the simulation time interval.

3. Numerical calculation and discussion

The typical values of parameters for 1550-nm InGaAsP–InP laser used in the simulations are given in Table 1. The nonlinear parameters, including ε_{N}, $\varepsilon_{\mathrm{ch}}$, $\varepsilon_{\mathrm{shb}}$, η^{N}, η^{ch}, η^1, τ_{ch}, and α_{ch}, are obtained by heterodyne detection methods for an SRL device.[18] The calculated threshold current for SRL in our simulation is 20 mA. The rate Eqs. (2) and (11) are solved numerically by means of the fourth-order Runge–Kutta method. The time interval is set to be as short as $\Delta t = 4$ ps. This small value corresponds to the Fourier white noise spectrum up to a frequency of 250 GHz ($1/\Delta t$), which

is much higher than the relaxation oscillation frequency (approximately 10 GHz). Moreover, this ensures enough resolution for the noise-induced spectrum characterization. In all of the integration process, we take $T = 10$, namely 21 modes for each direction of SRL (totally 42 modes).

We apply the model to the free-running SRL without any external feedback to investigate the dynamical mechanisms, including *L–I* curves, time-averaged frequency spectra, normalized temporal variations and corresponding RIN characteristics. Then, we will focus on the typical bi-AO and bis-UNI regimes of SRL to study the influence of the backscattering rate on RIN properties.

Table 1. Valus of parameters used in the numerical simulation.

Parameters	Symbol	Value
SRL cavity length	L/μm	405
Confinement factor	Γ	0.056
Internal loss	γ/cm^{-1}	10
Transparency carrier density	N_0/m^{-3}	2.32×10^{24}
Differential gain coefficient	a/m^2	6.35×10^{-20}
Linear gain dispersion coefficient	b_1/m^{-1}·m^{-2}	1.8×10^{18}
Linear gain dispersion coefficient	b_2/m^{-1}·m^{-2}	1.2×10^{18}
Nonrad. recombination coefficient	A/s^{-1}	1×10^{8}
Spont. recombination coefficient	B/m^3·s^{-1}	1.2×10^{-16}
Auger recombination coefficient	C/m^6·s^{-1}	7.5×10^{-41}
Group index	n_g	3.7
Refractive index of central mode	n_0	3.5
Nonlinear coefficient of CDP	ε_N/m^3	2.0×10^{-22}
Nonlinear coefficient of CH	ε_{ch}/m^3	1.91×10^{-24}
Nonlinear coefficient of SHB	ε_{shb}/m^3	1.76×10^{-24}
Differential carrier lifetime	τ_N/ns	0.5
Electron carrier heating time	τ_{ch}/ps	0.6
Intra-band relaxation time	τ_1/ps	0.1
Linewidth enhancement factor	α	3.56
Linewidth enhancement factor for CH	α_{ch}	2.0
conservative coupling rate	k_c	varied
dissipative coupling rate	k_d	4.5×10^7
Grating visibility for CDP	η^N	0.0036 / 1
Grating visibility for CH	η^{ch}	0.73 / 1
Grating visibility for SHB	η^1	0.95 / 1

3.1. *L–I* characteristics

The steady-state *L–I* curves for the SRL can be obtained by tracking the time domain response as the current increases. The injection current is varied in steps of $1/20I_{th}$, ranging from I_{th} to $7.5I_{th}$. Figure 2(a) shows the simulated *L–I* curves for both CW and CCW total optical powers and Fig. 2(b) presents the corresponding *L–I* curves for both CW and CCW separate optical field modes. From Fig. 2(a) we can observe the three working regimes of the SRL, bi-AO, bis-UNI and bidirectional unstable (bi-UNS) totally. The *L–I* curves in Fig. 2 are in good agreement with the experimental measurements,[4] which offers a potential guarantee for the following further noise characteristic analyses.

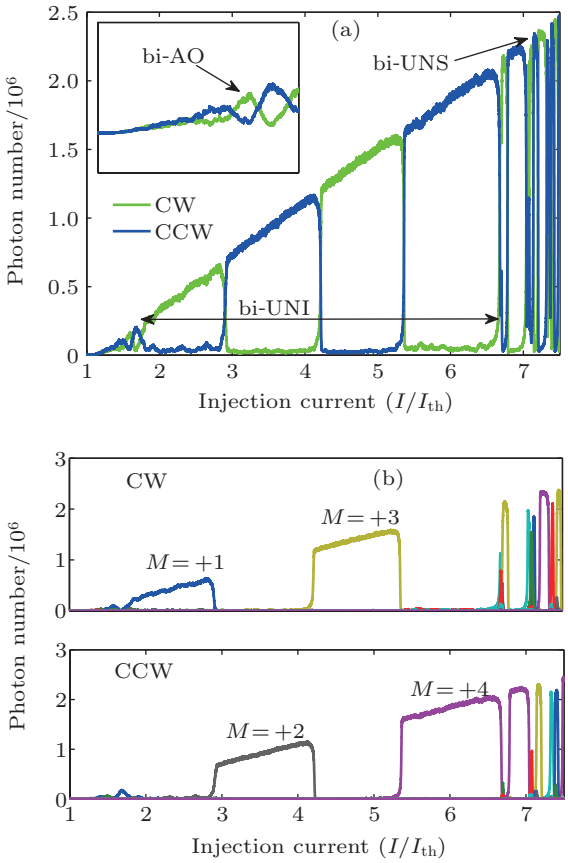


Fig. 2. (color online) Simulated *L–I* characteristics of an SRL showing (a) the total optical powers in both CW and CCW directions and the oscillation of photon numbers in both directions at the very beginning (in the inset), and (b) the separate optical field modes in both CW and CCW directions.

3.2. Multimode dynamics and RIN characteristics of SRLs

Just above the threshold current, the so-called bidirectional operating regime with alternate oscillation (bi-AO) is observed, where the output powers of both directions are periodically oscillating, which is attributed to the alternate oscillation between corresponding modes in counter-propagating directions. The oscillation behaviors of some main modes in both directions at $I = 1.5I_{th}$ are depicted in Fig. 3. The value of the mode photon number is taken after being normalized. As can be seen from it, when mode $M = +1$ (CW) reaches its maximum, the mode $M = +1$ (CCW) reaches its minimum and *vice versa*. Figure 4 shows the corresponding time-averaged optical spectra, from which we can find a conventional bidirectional multimode spectra due to the dominating amplified spontaneous emission (ASE) noise and asymmetric gain suppression resulting in the asymmetric gain spectra. When the current reaches $1.65I_{th}$, the power oscillation is only taken between the two main modes ($M = +1$ in the CW direction and the CCW direction) just as shown in Fig. 5, we call it the single-mode bi-AO regime to differentiate from the multimode bi-AO regime.

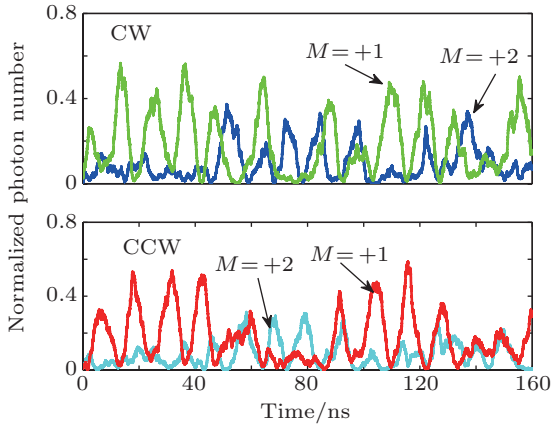


Fig. 3. (color online) Example of the simulation results of the SRL operating in the bi-AO regime with $I = 1.5I_{\rm th}$, showing the temporal variations of the normalized photon number of some main modes in both directions.

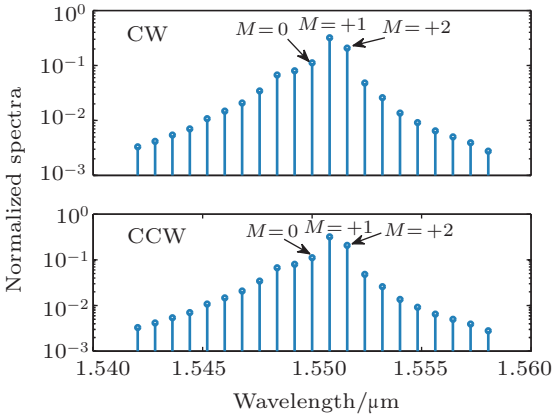


Fig. 4. (color online) Example of the simulation results of the SRL operating in the bi-AO regime with $I = 1.5I_{\rm th}$, showing the corresponding time-averaged optical spectra for both directions.

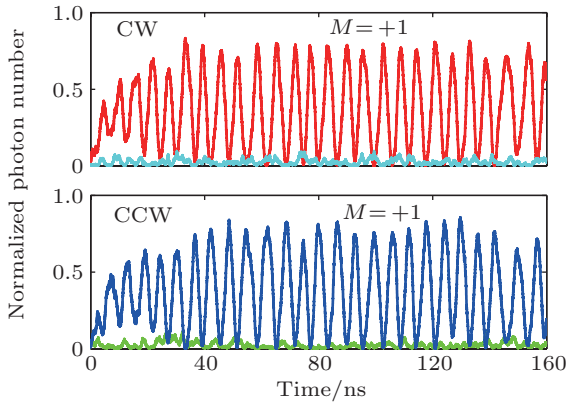


Fig. 5. (color online) Example of the simulation results of the SRL operating in the bi-AO regime with $I = 1.65I_{\rm th}$, showing temporal variations of the normalized photon number of the main modes in both directions.

The RIN spectra of the two bi-AO regimes are respectively depicted in Fig. 6. Just like in the case of a conventional semiconductor laser,[8,9] the pronounced relaxation oscillation peaks can be found around 7 GHz, which shift toward the higher frequency side with the increase of the injection current. This behavior is attributed to the increase of repetition of the output power fluctuation with the increase of current I. Compared with conventional semiconductor lasers, the SRL possesses a most remarkable feature of the RIN spectra which is the significant enhancement of low frequency RIN in the form of a broad low frequency tail extending all the way to the relaxation oscillation peak. The low frequency RIN of the multimode bi-AO regime at $I = 1.5I_{\rm th}$ is leveling off at 10^{-10} Hz^{-1}. When the SRL operates in the single-mode bi-AO regime, the low-frequency RIN level is almost one order of magnitude lower than in the single-mode bi-AO regime. A pronounced and sharp peak appears in the low-frequency region as shown in Fig. 10 at $f = 150$ MHz corresponding to the oscillating period $T = 1/f = 6.67$ ns in Fig. 5. The actual value of this frequency denotes the power exchange rate between the CW and CCW directions. The location of this low frequency peak is determined by the conservative backscattering coefficient, which will be discussed in the following section.

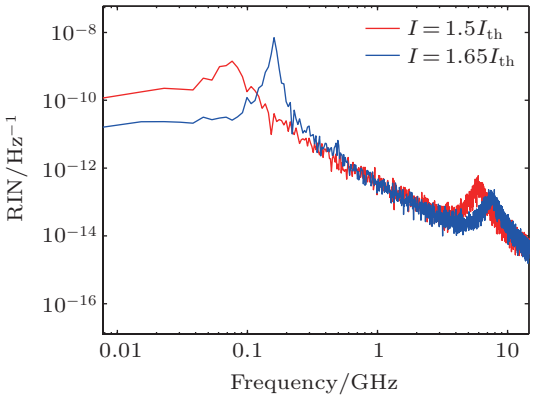


Fig. 6. (color online) The RIN spectra in the CCW direction of the SRL operating in the bi-AO regime. $k_{\rm d} = 4.5 \times 10^7$ and $k_{\rm c} = 5.2 \times 10^8$.

When the injection current increases from $1.7I_{\rm th}$ to $6.7I_{\rm th}$, the bistable unidirectional (bi-UNI) operating regime emerges, which is the dominant operation regime of the SRL. In this regime, the lasing direction changes as the injection current increases and the lasing mode hops to the long wavelength side at each jumping point correspondingly. The temporal variations and time-averaged spectra at $I = 35I_{\rm th}$ are illustrated in Figs. 7 and 8. The stable single longitudinal mode operation could be explicitly observed from these two figures; the main lasing mode has shifted from $M = +1$ (shown in Fig. 2(b)) to $M = +2$, which is attributed to the interaction between linear gain and asymmetric gain suppression. The side mode suppression ratio (SMSR) is more than 2 dB.

This distinct mode hopping phenomenon can be understood with the help of the optical spectra shown in Fig. 8. As is well known, asymmetric gain suppression inclines to enhance the modes on its long wavelength side and suppress the modes on its short wavelength side in both directions.[18] This can explain the asymmetric spectrum in the CW direc-

tion shown in Fig. 8. However, this effect is partly compensated by FWM, which has the opposite asymmetry with respect to wavelength,[18] i.e. it tends to enhance the modes on the shorter wavelength side. Unlike the asymmetric gain suppression that can occur between any modes in both directions, FWM can happen only among modes propagating in the same direction. This is responsible for the slightly asymmetric spectrum in the CCW direction. Therefore, mode $M = +3$ in the CW direction has the priority to be selected as a predominant lasing mode over CCW mode $M = +3$ in mode competition. Moreover, nonlinear effects are directly proportional to the intensity of the optical field determined by the injection current. Therefore, the mode hopping to the long wavelength of the opposite direction happens when the gain maximum shifts to the location of mode $M = +3$ as the current further increases. As can be verified from Fig. 2(b), the dominant lasing mode has shifted from CCW mode $M = +2$ to CW mode $M = +3$ in the higher current region.

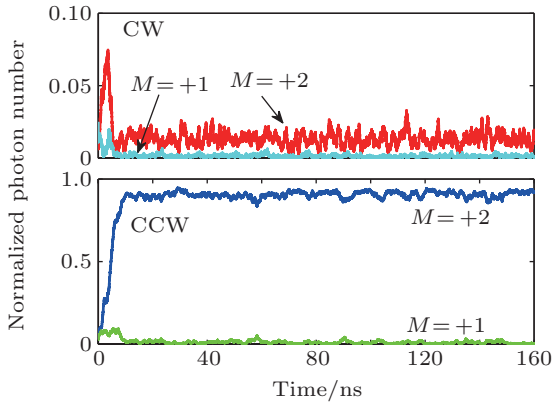


Fig. 7. (color online) Example of the simulation results of the SRL operating in the bis-UNI regime with $I = 3.5I_{\rm th}$, showing the temporal variations of the normalized photon number of some main modes in both directions.

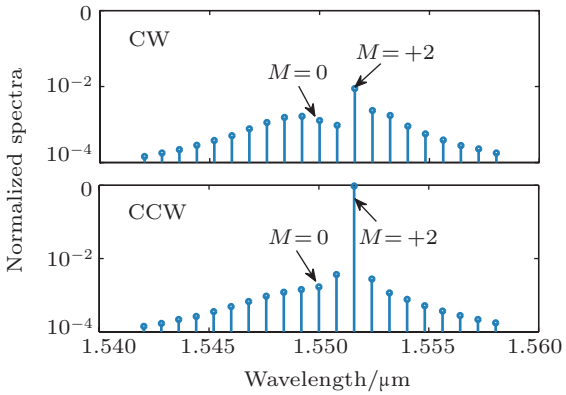


Fig. 8. (color online) Example of the simulation results of the SRL operating in the bis-UNI regime with $I = 3.5I_{\rm th}$, showing the corresponding time-averaged optical spectra for both directions.

The corresponding RIN spectra of the bis-UNI regime in SRL are shown in Fig. 9 and the RIN spectra of the bi-AO regime are also plotted for comparison. The relaxation oscillation peak shifts toward the higher frequency side due to the higher current $I = 3.5I_{\rm th}$. The broad enhanced low frequency RIN extends all the way to the relaxation oscillation peak with no pronounced peak appearing in the low-frequency region. The whole low-frequency RIN level drops off nearly two orders of magnitude than that in the multimode bi-AO regime.

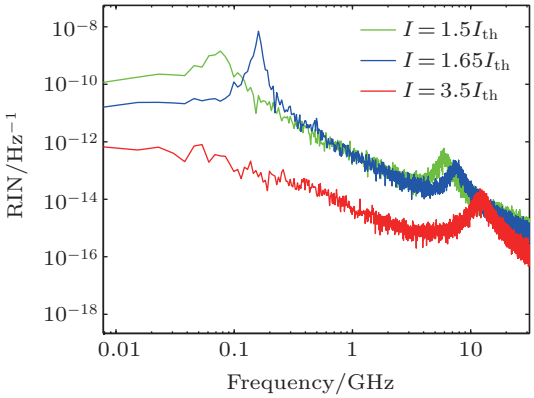


Fig. 9. (color online) The RIN spectra in the CCW direction of SRL operating in the bis-UNI regime and bi-AO regime. $k_{\rm d} = 4.5 \times 10^7$ and $k_{\rm c} = 5.2 \times 10^8$.

For the current above $6.7I_{\rm th}$, the bidirectional unstable (bi-UNS) regime or the regime of mode hopping with alternate oscillation could be observed, in which both the CW and CCW directions are unstable and the jumping frequency is relatively fast. Which mode in both directions would be the lasing mode could not be ruled, seemingly in a random way, as a result of the interaction between the asymmetric gain suppression and linear gain. The time traces of some main modes ($M = +2$ $+3$ $+4$ for CW and CCW) and time-averaged spectra are shown in Figs. 10 and 11. It is clear that mode hopping happens among the longitudinal modes propagating in both directions. It should be pointed out that even though the spectrum looks like a multimode operation due to a time averaged result, as shown in Fig. 4, the device actually lies in single mode operation between the mode hopping points.

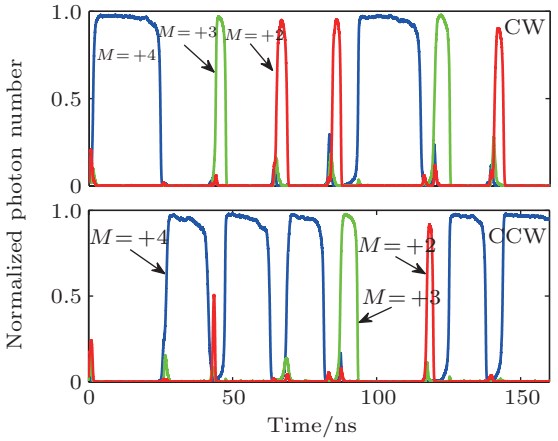


Fig. 10. (color online) Example of the simulation results of the SRL operating in the bi-UNS regime with $I = 7.2I_{\rm th}$, showing the temporal variations of the normalized photon number of some main modes in both directions.

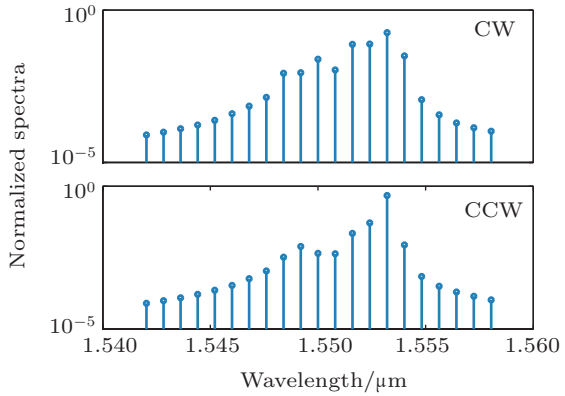


Fig. 11. (color online) Example of the simulation results of the SRL operating in the bi-UNS regime with $I = 7.2I_{\rm th}$, showing the corresponding time-averaged optical spectra for both directions.

The RIN spectra of the above mentioned bi-UNS regime are depicted in Fig. 12, along with the spectra of other regimes for comparison. The most remarkable feature of RIN spectrum in this regime is the great enhancement of low frequency RIN, which causes the relaxation oscillation peak to become unapparent. The RIN level in the bi-UNS regime is the highest in the three operating regimes. Furthermore, another peak approximately at 80 MHz attributed to the mode hopping phenomenon between the CW and CCW directions could be observed in the bi-UNS regime. The mode hopping is caused greatly by the backscattering coupling and nonlinear mechanisms introduced into the rate Eq. (2), especially the asymmetric contribution of CDP and CH effects.[18] The location of this peak greatly depends on the backscattering coefficient and the drive current. Experimental demonstration of this enhanced low frequency noise in 1550-nm ridge waveguide InGaAsP–InP SRL has already been performed in Ref. [23].

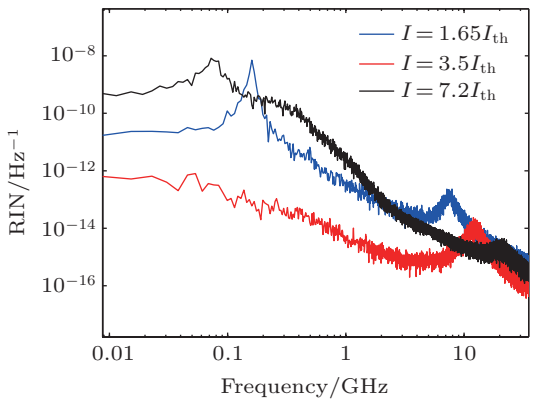


Fig. 12. (color online) The respective RIN spectra of CCW direction for the above-mentioned three kinds of operating regimes of SRL. $k_{\rm d} = 4.5 \times 10^7$ and $k_{\rm c} = 5.2 \times 10^8$.

3.3. Influence of intra-cavity backscattering on RIN characteristics

The intra-cavity backscattering coefficients are important to determine the static and dynamic properties of SRLs. Physically, the backscattering coefficient represents the energy exchange rate between the two directions. The actual values for $k_{\rm c}$ and $k_{\rm d}$ are determined by localized and distributed variations of the refractive index and the loss of the passive ring cavity.[3] The light extraction port in SRL introduces a perturbation of the refraction index, which turns out to be a localized reflection enhancing the conservative coefficient. Therefore, the SRL is subjected to the conservative backscattering much more than the dissipative one. Moreover, the conservative coefficient plays a dominant role in determining the operating regime of SRL. So we will focus on the influence of conservative backscattering coefficient on the RIN characteristics in the bi-AO and bis-UNI regimes. These two regimes are much more useful and attractive in the actual OEIC systems based on SRLs.[6,7]

Figure 13 shows how the RIN spectrum is modified by the conservative backscattering coefficient in the single-mode bi-AO regime. The resonance peak shifts towards the higher frequency side and is much sharper with the increase of conservative coupling rate $k_{\rm c}$, while the low-frequency RIN level is inversely related to the $k_{\rm c}$. Such behaviors are in good agreement with the work done by Antonio *et al.*[15] The spectra are in good accordance with each other in the high frequency domain, which implies that the conservative backscattering coefficient has no influence on the high frequency domain of RIN.

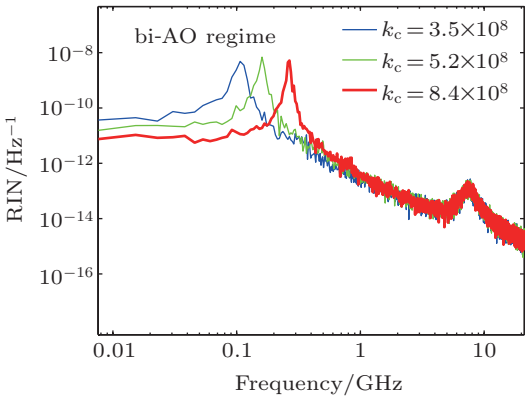


Fig. 13. (color online) RIN spectra of CCW direction in the bi-AO regime, showing their dependence on the conservative backscattering coefficient $k_{\rm c}$. Here $k_{\rm d} = 4.5 \times 10^7$ and $I = 1.65I_{\rm th}$.

When the SRL works in the bis-UNI regime, the corresponding RIN spectrum dependence on the conservative backscattering coefficient is depicted in Fig. 14. Just as the case in Fig. 13, the RIN spectra are in good accordance with each other in the high frequency domain, which again verifies the insensitivity of high frequency RIN to the backscattering coefficient. The low-frequency RIN level drops off gradually with the decrease of the conservative backscattering rate, which is different from the case in the bi-AO regime.

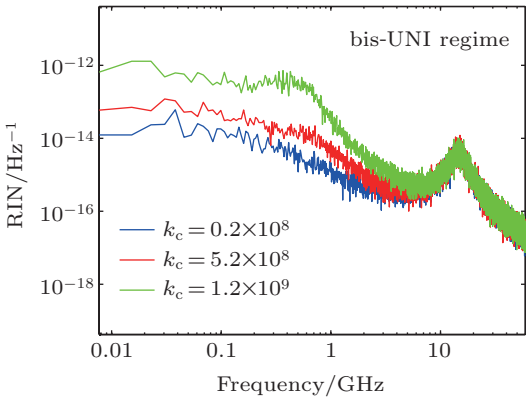


Fig. 14. (color online) RIN spectra of CCW direction in the bis-UNI regime, showing their dependences on conservative backscattering coefficient k_c. Here $k_d = 4.5 \times 10^7$ and $I = 4I_{th}$.

4. Conclusions

A novel frequency domain multimode model is employed to investigate the multimode dynamics and RIN characteristics of SRLs. The comprehensive nonlinear mechanisms among the lasing modes, such as SHB, CH, and CDP effects, are introduced into this model. Additionally, the Langevin noise sources on electric field and carrier density fluctuation are also taken into account. Different operation regimes are observed, i.e. the bidirectional operation with alternate oscillations just above the threshold current, the bistable unidirectional operating regime that emerges with a moderate injection current and the bidirectional unstable regime with a higher current.

Compared with the case of a conventional FP laser, a most remarkable feature of the RIN spectrum is the significant enhancement of low frequency RIN in the form of a broad low frequency tail extending all the way to the relaxation oscillation peak in any regime of the SRLs. The conservative backscattering coefficient significantly affects the performances of OEIC systems based on SRLs. Therefore, the influences of this particular parameter on the RIN properties are investigated in detail in the typical bi-AO and bis-UNI regimes of SRLs.

References

[1] Thomas L K and Uziel K 1991 *IEEE J. Quantum Electron.* **27** 641
[2] Chen C, Zhao L J, Qiu J F, Liu Y, Wang W and Lou C Y 2012 *Chin. Phys. B* **21** 094208
[3] Sorel M, Giuliani G, Scire A, Miglierina R, Donati S and Laybourn P J R 2003 *IEEE J. Quantum Electron.* **39** 1187
[4] Sorel M, Laybourn P J R, Scire A, Balle S and Donati S 2002 *Opt. Lett.* **27** 1992
[5] Cai X L, Daniel H Y L, Gábor M, Wang Z R, Sorel M and Yu S Y 2012 *IEEE J. Quantum Electron.* **48** 406
[6] Pérez T, Scirè A, Van der Sande G, Colet P and Mirasso C R 2007 *Opt. Express* **15** 12941
[7] Thakulsukanant K, Li B, Memon I and Yu S Y 2009 *IEEE J. Lightwave Technol.* **27** 631
[8] Ahmed M, Yamada M and Saito M 2001 *IEEE J. Quantum Electron.* **37** 1600
[9] Wang A B, Wang Y C, Yang Y B, Zhang M J and Wang B J 2013 *Appl. Phys. Lett.* **102** 031112
[10] Xie H Y, Pan J Q, Zhao L J, Zhu H L, Wang L F and Wang W 2006 *Chin. Phys. Lett.* **23** 126
[11] Ji C, Booth M F, Schremer A T and Ballantyne J M 2005 *IEEE J. Quantum Electron.* **41** 925
[12] Stamataki I, Mikroulis S, Kapsalis A and Syvridis D 2006 *IEEE J. Quantum Electron.* **42** 1266
[13] Yamada M and Suematsu Y 1981 *J. Appl. Phys.* **52** 2653
[14] Yamada M 1989 *J. Appl. Phys.* **66** 81
[15] Antonio P S, Zambrini R, Scirè A and Colet P 2009 *Phys. Rev. A* **80** 043843
[16] Born C, Yuan G H, Wang Z R and Yu S Y 2008 *IEEE J. Quantum Electron.* **44** 1055
[17] Uskov A, Mork J and Mark J 1994 *IEEE J. Quantum Electron.* **30** 1769
[18] Born C, Sorel M and Yu S Y 2005 *IEEE J. Quantum Electron.* **41** 261
[19] Ahmed M, Mahmoud S W Z and Yamada M 2007 *Int. J. Numer. Model.* **20** 117
[20] Sazzad M S I, Yamada M and Kuwamura Y J 2012 *IEEE J. Quantum Electron.* **48** 521
[21] Coldren L A and Corzine S W 1995 *Diode Lasers and Photonic Integrated Circuits* (New York: Wiley)
[22] Haug H 1969 *Phys. Rev.* **184** 338
[23] Mikroulis S, Stamataki I, Hamacher M, Roditi E and Syvridis D 2006 *IEEE Photon. Technol. Lett.* **18** 1895